Journal of Applied Physics

Topological honeycomb magnon Hall effect: A calculation of thermal Hall conductivity of magnetic spin excitations

Cite as: J. Appl. Phys. **120**, 043903 (2016); https://doi.org/10.1063/1.4959815
Submitted: 13 May 2016 . Accepted: 14 July 2016 . Published Online: 25 July 2016

S. A. Owerre

Topological honeycomb magnon Hall effect: A calculation of thermal Hall conductivity of magnetic spin excitations

S. A. Owerre[a)]
African Institute for Mathematical Sciences, 6 Melrose Road, Muizenberg, Cape Town 7945, South Africa and Perimeter Institute for Theoretical Physics, 31 Caroline St. N., Waterloo, Ontario N2L 2Y5, Canada

(Received 13 May 2016; accepted 14 July 2016; published online 25 July 2016)

Quite recently, the magnon Hall effect of spin excitations has been observed experimentally on the kagome and pyrochlore lattices. The thermal Hall conductivity κ^{xy} changes sign as a function of magnetic field or temperature on the kagome lattice, and κ^{xy} changes sign upon reversing the sign of the magnetic field on the pyrochlore lattice. Motivated by these recent exciting experimental observations, we theoretically propose a simple realization of the magnon Hall effect in a two-band model on the honeycomb lattice. The magnon Hall effect of spin excitations arises in the usual way via the breaking of inversion symmetry of the lattice, however, by a next-nearest-neighbour Dzyaloshinsky-Moriya interaction. We find that κ^{xy} has a fixed sign for all parameter regimes considered. These results are in contrast to the Lieb, kagome, and pyrochlore lattices. We further show that the low-temperature dependence on the magnon Hall conductivity follows a T^2 law, as opposed to the kagome and pyrochlore lattices. These results suggest an experimental procedure to measure thermal Hall conductivity within a class of 2D honeycomb quantum magnets and ultracold atoms trapped in a honeycomb optical lattice. *Published by AIP Publishing.*
[http://dx.doi.org/10.1063/1.4959815]

INTRODUCTION

In recent years, the understanding of the topological nature of phonons and magnons in quantum materials has been at the pinnacle of intense investigation. These materials are believed to be applicable to many technological systems such as thermal devices and spintronics. The most fascinating property of these materials is the observation of thermal Hall effect, which occurs at finite temperature. Phonon Hall effect has been observed experimentally in $Tb_3Ga_5O_{12}$,[1] and the topological properties have been studied in terms of the Berry curvature of the system in different lattice geometries.[2,3] Recently, the topological properties of magnons in quantum magnets[4–8] have become a subject of interest because of the possibility of thermal Hall effect characterized by a nonzero thermal Hall conductivity κ^{xy}, at finite temperature. The thermal Hall effect in quantum magnets was first predicted theoretically by Katsura *et al.*[4] on the kagome and pyrochlore ferromagnets with a nearest-neighbour (NN) Dzyaloshinsky-Moriya (DM) interaction.[9] It was later discovered experimentally by Onose *et al.*[5] in the ferromagnetic insulator $Lu_2V_2O_7$ on a three-dimensional (3D) pyrochlore lattice. Subsequently, Matsumoto and Murakami[6] relate κ^{xy} directly to the Berry curvature of the magnon bulk bands reminiscent of Hall conductivity in electronic systems.[10] This result shows that at nonzero temperature, $\kappa^{xy} \neq 0$ provided that the magnon bulk bands have a nontrivial gap at the Dirac points, i.e., the points where two bands touch in the Brillouin zone.

It has also been shown that κ^{xy} changes sign as a function of temperature or magnetic field.[11,12] Also recently, the thermal Hall effect has been observed experimentally on the 2D kagome magnet Cu(1–3, bdc),[13] thus opening a wide spectrum of research to search for topological magnon insulators in 2D quantum magnets. In both 2D kagome magnets and 3D pyrochlore magnets, the breaking of inversion symmetry by a NN DM interaction plays a crucial role. The DM interaction introduces a spin-orbit coupling, as a result, the bosons accumulate a phase as they hop through the lattice sites, reminiscent of the Haldane model in electronic systems.[14] Thus far, the thermal Hall effect in quantum magnets has been studied only in three lattice geometries—the three magnon bulk bands of kagome lattice,[4,11–13] the four magnon bulk bands of pyrochlore lattice,[5,6] and three magnon bulk bands of Lieb lattice.[15] However, a topological magnon insulator is also realizable in a two-band honeycomb ferromagnetic model.[16]

The purpose of this paper is to provide a simple theoretical realization of the magnon Hall effect in this two-band model on the honeycomb lattice. In this system, a nontrivial magnon bulk gap arises in the presence of a next-nearest-neighbour (NNN) DM interaction as opposed to the kagome and the pyrochlore lattices.[4–6,12,13] We explicitly demonstrate the theory of thermal Hall effect in this system. We find that κ^{xy} in this system has a fixed sign for all values of the parameters considered at finite temperatures. In contrast to 2D kagome and 3D pyrochlore lattices, we also find that the low-temperature dependence on the magnon Hall conductivity is $\propto T^2$. The model studied here can be mapped to hardcore bosons on the honeycomb lattice with Haldane-like NNN hopping. In fact, a recent study has reported an experimental realization of the Haldane model using ultracold fermionic atoms in a periodically modulated optical honeycomb lattice.[17] Thus, the results obtained in this paper suggest an experimental procedure to search a bosonic

a)solomon@aims.ac.za

analogue of the Haldane model in 2D honeycomb quantum magnets and ultracold atoms trapped in the honeycomb optical lattice.

TWO-BAND HONEYCOMB FERROMAGNETIC MODEL

In a recent study, the author has shown the first existence of topological magnon insulator on the honeycomb lattice with two-magnon bands.[16] In this paper, we provide the first evidence of the thermal Hall effect of magnetic spin excitations in this model, governed by the Hamiltonian[16]

$$H = -J\sum_{\langle ij\rangle}\mathbf{S}_i\cdot\mathbf{S}_j - J'\sum_{\langle\langle ij\rangle\rangle}\mathbf{S}_i\cdot\mathbf{S}_j + \sum_{\langle\langle ij\rangle\rangle}\mathbf{D}_{ij}\cdot\mathbf{S}_i\times\mathbf{S}_j - h\sum_i S_i^z. \tag{1}$$

The first two terms are ferromagnetic Heisenberg exchange couplings on the NN sites $J>0$ and NNN sites $J'>0$, respectively. The third term is a NNN DM interaction between sites i and j. The DM interaction generates a magnetic flux. Figure 1 shows the direction of the magnetic flux generated by the DM interaction on the unit cells with $\mathbf{D}_{ij} = \nu_{ij}\mathbf{D}\cdot\hat{z}$, where $\nu_{ij} = \pm 1$ for hopping from left to right and vice versa. Thus, the NNN DM interaction plays the role of spin-orbit coupling and breaks the inversion symmetry of the lattice. The last term is the Zeeman magnetic field with $h = g\mu_B B$ being the magnetic field strength, g is the spin g-factor, and μ_B is the Bohr magneton. Notice that this system is a ferromagnetic insulator despite the presence of the DM interaction.

It is well-known that the physics of thermal Hall effect can be understood entirely by semiclassical methods.[4–6,12] Recent experimental results on the kagome ferromagnet[13] suggest that the Holstein Primakoff transformation is a better predictor than the Schwinger boson representation. Using the former method, the spin Hamiltonian maps to a bosonic tight binding hopping model given by

$$H = -v_s\sum_{\langle ij\rangle}(b_i^\dagger b_j + h.c.) - v_t\sum_{\langle\langle ij\rangle\rangle}(e^{i\phi_{ij}}b_i^\dagger b_j + h.c.) + v_0\sum_i b_i^\dagger b_i, \tag{2}$$

where $v_0 = (zv_s + z'v_s' + h)$, $v_t = \sqrt{v_s'^2 + v_D^2}$, $v_s(v_s')(v_D) = JS(J'S)(DS)$, and $z(z') = 3(6)$ are the number of NN and NNN sites, respectively. We have assumed a DM interaction along the z-quantization axis. As a result of the DM interaction, the bosons accumulate a phase $\phi_{ij} = \nu_{ij}\phi$, where $\phi = \arctan(D/J')$ is a magnetic flux generated by the DM interaction on the NNN sites, similar to the Haldane model with $\nu_{ij} = \pm 1$ as in electronic systems.[14] The momentum space Hamiltonian is given by $H = \sum_{\mathbf{k}}\Psi_{\mathbf{k}}^\dagger\cdot\mathcal{H}_B(\mathbf{k})\cdot\Psi_{\mathbf{k}}$, where $\Psi_{\mathbf{k}}^\dagger = (b_{\mathbf{k}A}^\dagger, b_{\mathbf{k}B}^\dagger)$, and the Bogoliubov Hamiltonian is given by

$$\mathcal{H}_B(\mathbf{k}) = h_0(\mathbf{k})\sigma_0 + h_x(\mathbf{k})\sigma_x + h_y(\mathbf{k})\sigma_y + h_z(\mathbf{k})\sigma_z, \tag{3}$$

where $h_0 = v_0 - 2v_t\cos\phi p_{\mathbf{k}}$, $h_x = -v_s\sum_\mu\cos\mathbf{k}\cdot\boldsymbol{\delta}_\mu$, $h_y = -v_s\sum_\mu\sin\mathbf{k}\cdot\boldsymbol{\delta}_\mu$, and $h_z = 2v_t\sin\phi\rho_{\mathbf{k}}$, where $p_{\mathbf{k}} = \sum_\mu\cos\mathbf{k}\cdot\boldsymbol{a}_\mu$ and $\rho_{\mathbf{k}} = \sum_\mu\sin\mathbf{k}\cdot\boldsymbol{a}_\mu$, and $\boldsymbol{\delta}_\mu$ are the three NN vectors on the honeycomb lattice given by $\boldsymbol{\delta}_1 = a(\sqrt{3}\hat{x},\hat{y})/2$, $\boldsymbol{\delta}_2 = a(-\sqrt{3}\hat{x},\hat{y})/2$, and $\boldsymbol{\delta}_3 = a(0,-\hat{y})$. The NNN vectors are shown in Fig. 1. The corresponding eigenvalues of Eq. (3) are given by

$$\epsilon_\lambda(\mathbf{k}) = h_0(\mathbf{k}) + \lambda\sqrt{h_x(\mathbf{k})^2 + h_y(\mathbf{k})^2 + h_z(\mathbf{k})^2} = h_0(\mathbf{k}) + \lambda\epsilon(\mathbf{k}), \tag{4}$$

where $\lambda = \pm$ labels the top and the bottom bands, respectively. The explicit form of the eigenvectors is given by

$$|\psi_\lambda(\mathbf{k})\rangle = \frac{1}{\sqrt{2}}\left(\sqrt{1+\lambda\frac{h_z(\mathbf{k})}{\epsilon(\mathbf{k})}},\quad -\lambda e^{-i\Phi(\mathbf{k})}\sqrt{1-\lambda\frac{h_z(\mathbf{k})}{\epsilon(\mathbf{k})}}\right)^T, \tag{5}$$

where

$$\tan\Phi(\mathbf{k}) = \frac{h_y(\mathbf{k})}{h_x(\mathbf{k})}. \tag{6}$$

As previously shown,[16,18] for $v_D = 0$ the system is gapless at two inequivalent Dirac points $\mathbf{K}_\pm = \pm\frac{4\pi}{3\sqrt{3}a}\hat{x}$. The NNN interaction J' and the magnetic field h only shift the energy of the Dirac points but do not open a gap. The gapless Dirac points have been shown to be robust against higher order magnon-magnon interactions.[18] As shown in Fig. 2, a gap

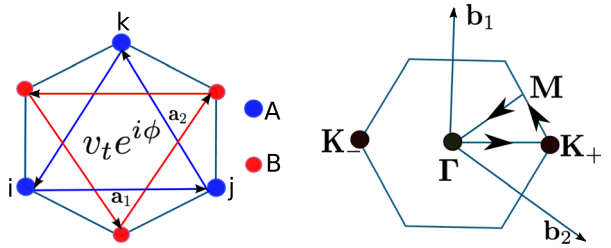

FIG. 1. (Left) The unit cell of the honeycomb lattice. The primitive lattice vectors are $\mathbf{a}_1 = \sqrt{3}a\hat{x}$; $\mathbf{a}_2 = a(-\sqrt{3}\hat{x},3\hat{y})/2$. The arrows show the treads of the magnetic flux generated by the DM interaction, $\mathbf{D}_{ij} = \nu_{ij}\mathbf{D}\cdot\hat{z}$, $v_t = S\sqrt{J'^2+D^2}$, and $\phi = \arctan(D/J')$. (Right) The Brillouin zone with reciprocal lattice vectors $\mathbf{b}_1 = 4\pi/3a\hat{y}$ and $\mathbf{b}_2 = 2\pi(\hat{x},-\hat{y}/\sqrt{3})/\sqrt{3}a$.

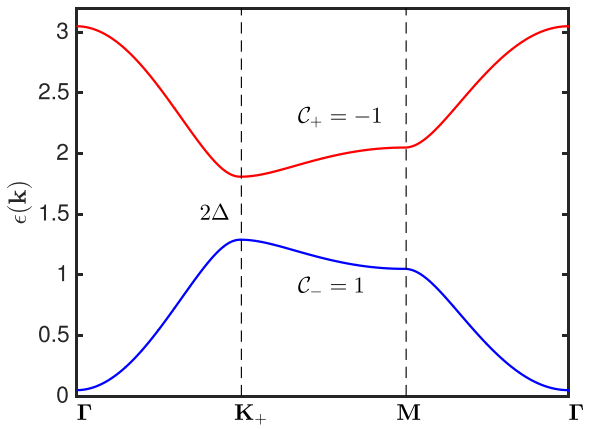

FIG. 2. Magnon bulk bands for the spin 1/2 honeycomb topological magnon insulator in units of $g = J = 1$ and the corresponding Chern numbers (see text for explanation) at $\mu_B B = 0.1$, $J' = D = 0.1J$, $\phi = \pi/4$. The gap at $\mathbf{K}_\pm$ is $\Delta = |h_z(\mathbf{k})| = 3\sqrt{3}v_t\sin\phi = 3\sqrt{3}v_D$. The NNN isotropic interaction does not contribute to gap opening. The gap at Γ is h.

only opens when $v_D \neq 0$, thus gives rise to nonzero Chern numbers defined below.

BERRY CURVATURE AND CHERN NUMBER

In fermionic systems, nontrivial band topology arises from the structure of the energy bands. This is characterized by a nonzero Berry curvature defined via the eigenstates of the system, which gives rise to a quantized integer (when the Fermi energy lies between the energy gaps) called the Chern number. In bosonic systems, the idea is essentially the same. A nontrivial band topology arises only when the system exhibits a nontrivial gap in the spin wave excitation spectra and a nonzero Chern number simply predicts the existence of edge state modes in the system. In 2D lattices, the Berry curvature is generally given by

$$\Omega_\lambda(\mathbf{k}) = -2\mathrm{Im}[\langle\partial_{k_x}\psi_\lambda(\mathbf{k})|\partial_{k_y}\psi_\lambda(\mathbf{k})\rangle]. \tag{7}$$

In the present model, the eigenstates are given in Eq. (5), hence we obtain

$$\Omega_\lambda(\mathbf{k}) = \frac{1}{2}\lambda\epsilon_{\mu\nu}\partial_{k_\mu}\phi(\mathbf{k})\partial_{k_\nu}\left(\frac{h_z(\mathbf{k})}{\epsilon(\mathbf{k})}\right), \tag{8}$$

where $\epsilon_{\mu\nu}$ is a 2D antisymmetric tensor.

The Berry curvature has two important properties. First, it is controlled by the mass gap at the Dirac points and the Chern number

$$\mathcal{C}_\lambda = \frac{1}{2\pi}\int_{BZ} d^2k\,\Omega_\lambda(\mathbf{k}), \tag{9}$$

of a gapless system $v_D = 0$ vanishes. Second, for a gapped system $v_D \neq 0$, the maximum contribution to the Chern number comes from the states near $\mathbf{K}_\pm$, i.e., when $\Delta = |h_z(\mathbf{k})| \to 0$, also the total Chern number vanishes. Therefore, no magnon edge state exists above the upper band.[16]

MAGNON HALL EFFECT

The nontrivial topology of the Berry curvatures leads to magnon edge states.[16] Interestingly, the magnon edge states carry a transverse heat (spin) current upon the application of a longitudinal temperature gradient. As magnons are uncharged particles, there is no Lorentz force, the DM interaction plays the role of an effective magnetic field by altering the propagation of the magnon in the system, thus leads to the magnon Hall effect.[5] In the following, we demonstrate how the topological nature of this system is manifested by computing important experimental observables. The important quantity characterizing the magnon Hall effect is the thermal Hall conductivity. Similar to Hall conductivity in electronic systems, the thermal Hall conductivity is related to the Berry curvature of the eigenstates. There are two contributions to the thermal conductivity given by[6]

$$\kappa_E^{xy} = -\frac{2}{T}\mathrm{Im}\sum_{\lambda=\pm}\int_{BZ}\frac{d^2k}{(2\pi)^2}n_B[\epsilon_\lambda(\mathbf{k})] \times\left[\langle\partial_{k_x}\psi_\lambda(\mathbf{k})|(\mathcal{H}_B(\mathbf{k})+\epsilon_\lambda(\mathbf{k}))^2|\partial_{k_y}\psi_\lambda(\mathbf{k})\rangle\right], \tag{10}$$

and

$$\kappa_O^{xy} = -\kappa_E^{xy} - \frac{k_B^2T}{(2\pi)^2}\sum_{\lambda=\pm}\int_{BZ} d^2k c_2(n_\lambda)\Omega_\lambda(\mathbf{k}), \tag{11}$$

where $n_\lambda \equiv n_B[\epsilon_\lambda(\mathbf{k})] = [e^{\epsilon_\lambda(\mathbf{k})/k_BT}-1]^{-1}$ is the Bose function, $c_2(x) = (1+x)\left(\ln\frac{1+x}{x}\right)^2 - (\ln x)^2 - 2\mathrm{Li}_2(-x)$, and $\mathrm{Li}_n(x)$ is a polylogarithm. The first contribution originates from the current density,[4] and the second contribution stems from the orbital motions of magnons.[6] Hence, the total contribution is given by

$$\kappa^{xy} = \kappa_E^{xy} + \kappa_O^{xy} = -\frac{k_B^2T}{(2\pi)^2}\sum_{\lambda=\pm}\int_{BZ} d^2k c_2(n_\lambda)\Omega_\lambda(\mathbf{k}). \tag{12}$$

It is evident that the thermal Hall conductivity is the Berry curvature weighed by the $c_2(n_\lambda)$ function. It depends on the existence of a nontrivial gap in the magnon bulk bands at $T \neq 0$. The largest contribution to κ^{xy} comes from the states near $\mathbf{K}_\pm$ due to the Berry curvature as mentioned above. In what follows, we apply Eq. (12) to the two-band model and we assume units such that $J = k_B = \hbar = 1$.

Figures 3(a) and 3(b) show the plot of T vs. $\kappa^{xy}(T)$ and $logT$ vs. $\log[-\kappa^{xy}(T)]$, respectively, and Figs. 4(a) and 4(b) show the contour plots of κ^{xy} in J'/J vs. D/J plane and μ_BB vs. T plane, respectively. We observe no sign change in κ^{xy} for all parameter regimes considered. This can be understood directly from Eq. (12). Since the Berry curvatures are equal and opposite $\Omega_+ = -\Omega_-$, Eq. (12) involves the difference between the $c_2[n(\epsilon_\lambda, T)]$ functions. At low temperatures, the lower band dominates, but due to the fact that $c_2[n(\epsilon_-, T)] > 0$ and $\Omega_- > 0$ for all parameter regimes, the thermal Hall conductivity is

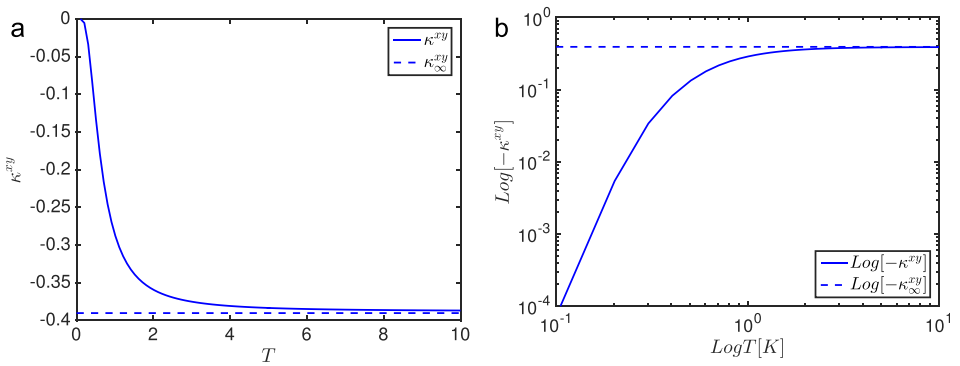

FIG. 3. The plot of (a) T vs. κ^{xy}; (b) $\log[T]$ vs. $\log[-\kappa^{xy}]$ with the same parameters in Fig. 2.

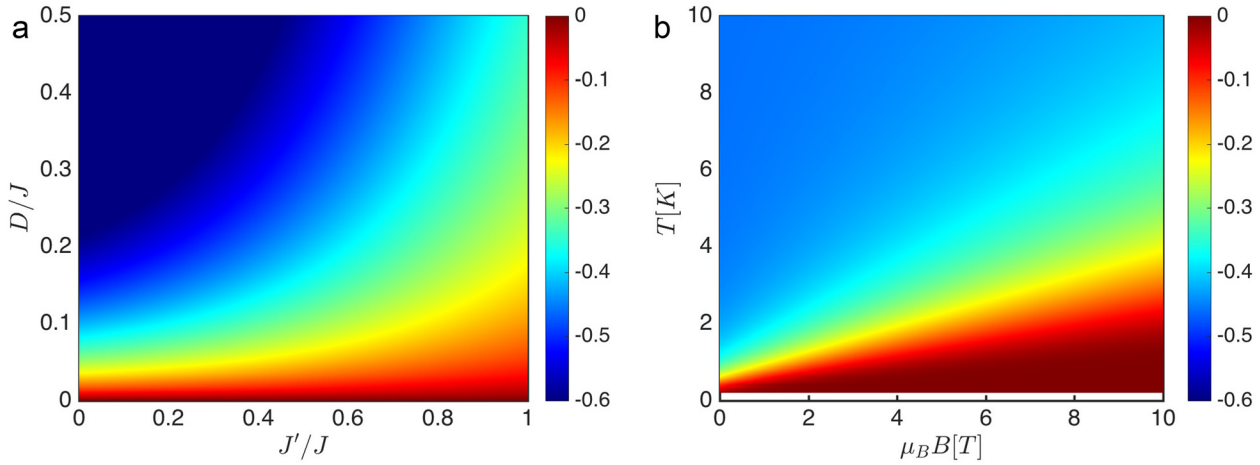

FIG. 4. The contour plot of κ^{xy} in the (a) D/J vs. J'/J plane at $T=1.5$ and $\mu_B B=0.1$. (b) $\mu_B B$ vs. T plane with the parameters in Fig. 2.

negative, $\kappa^{xy}<0$, in the low-T limit. At high temperatures, the $T\to\infty$ limit of $\kappa^{xy}(T)$ is given by[12]

$$\kappa^{xy}_{\infty}=\frac{k_B^2}{(2\pi)^2}\sum_{\lambda=\pm}\int_{BZ}d^2k\epsilon_\lambda\Omega_\lambda(\mathbf{k}). \tag{13}$$

In Fig. 5, we show the integrand in Eq. (13) describing the high-temperature limit of the thermal Hall conductivity. As mentioned above, it is obvious that the dominant contribution comes from the Dirac points $\mathbf{K}_\pm$. Because of the fact that $\epsilon_+>\epsilon_-$, the integrand is dominated by the upper band, but since $\Omega_+=-\Omega_-<0$ the integrand is negative. Again $\kappa^{xy}_{\infty}<0$ as shown in Figs. 3(a) and 3(b). Therefore, the high and low temperature limits of $\kappa^{xy}(T)$ have the same sign. The sign of κ^{xy} is inherited from the topology of the magnon bulk bands. For the kagome lattice, Ref. 11 explains the sign change in κ^{xy} as a consequence of the sign change in Berry curvature of the highest band, and Ref. 12 argues that the sign change in κ^{xy} is a consequence of the propagation of the magnon edge states, however, with a NNN interaction. The origin of the sign change on the kagome[4,11,12] and Lieb[15] ferromagnets is still not well-understood theoretically. Since both lattices have a flat band, it may be possible that this flat band has an effect on the nature of the thermal conductivity.

Next, we calculate the explicit form of the low-temperature dependence of Eq. (10). As mentioned above,

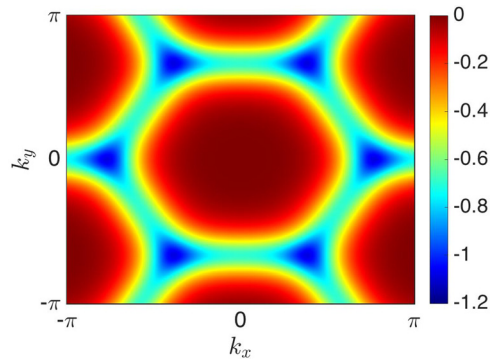

FIG. 5. The integrand $\sum_{\lambda=\pm}\epsilon_\lambda\Omega_\lambda(\mathbf{k})$ in Eq. (13) describing the high-temperature limit of the thermal Hall conductivity. The parameters are the same as in Fig. 2.

the lower band dominates at low temperature. Inserting a complete set of states into Eq. (10) gives[5]

$$\kappa^{xy}_{E}\sim\frac{1}{T}\int\frac{d^2k}{(2\pi)^2}n_B[\epsilon_-(\mathbf{k})]\big(\epsilon_-(\mathbf{k})+\epsilon_+(\mathbf{k})\big)^2\Omega_-(\mathbf{k}). \tag{14}$$

The dominant contribution comes from the $\mathbf{k}=0$ mode. Near $\mathbf{k}=0$, $\epsilon_-(\mathbf{k})+\epsilon_+(\mathbf{k})\sim 2(h+3v_s)$ and $\epsilon_-(\mathbf{k})\sim h+\frac{3v_s}{4}k^2$. Since the Berry curvature $\Omega_-(\mathbf{k})$ vanishes at $\mathbf{k}=0$, we must expand it to quadratic order. The denominator is finite at $\mathbf{k}=0$, so we expand the numerator as $\mathbf{k}\to 0$. The only non-zero term in the expansion up to quadratic order is given by

$$\Omega_-(\mathbf{k})\sim\alpha k_x^2k_y^2, \tag{15}$$

where $\alpha=3\sqrt{3}v_t\sin\phi/32v_s$. Performing the angular part of the integration, Eq. (14) takes the form

$$\begin{aligned}\kappa^{xy}_{E}&\sim\frac{\alpha(h+3v_s)^2}{4\pi T}\int_0^\infty k\,dk\,\frac{k^4}{e^{\left(h+\frac{3v_s}{4}k^2\right)/T}-1},\\&=\left(\frac{T}{v_s^2}\right)^2\frac{v_t\sin\phi(h+3v_s)^2}{6\sqrt{3}\pi}\mathrm{Li}_3\left[\exp\left(-\frac{h}{T}\right)\right].\end{aligned} \tag{16}$$

This expression [Eq. (16)] shows that the honeycomb chiral ferromagnet has a different feature from the kagome and pyrochlore lattices.[4,5]

CONCLUSION

The main result of this paper is that the magnon Hall effect is realizable in a two-band model on the honeycomb lattice. In this paper, we have shown that the thermal Hall conductivity on the honeycomb lattice does not change sign as the temperature or magnetic field vary, with other parameters fixed. We also showed that the low-temperature dependence on the thermal Hall conductivity is also different from the kagome and pyrochlore lattices and follows the relation: $\kappa^{xy}_{E}\propto T^2$. As previously mentioned, the model studied is related to hard-core bosons, and the resulting Hamiltonian is analogous to the Haldane model in electronic systems. Hence, the magnon Hall effect on the honeycomb lattice

could be accessible using ultracold bosonic atoms trapped in the honeycomb optical lattice. Although honeycomb ferromagnets are difficult to find in nature, they exist in intra-layer regions in some materials and can be considered as two-dimensional materials if the intra-layer coupling, say, J_t is larger than the inter-layer coupling, say, J_l. This is the case in the crystal $CrBr_3$, which comprises a strong nearest-neighbour honeycomb ferromagnetic intra-layer coupling.[19,20] It might be possible to induce a DM interaction in this ferromagnetic material and the results of this paper can be confirmed directly. This might also be applicable to the field of spintronics.

ACKNOWLEDGMENTS

The author would like to thank the African Institute for Mathematical Sciences (AIMS). Research at Perimeter Institute was supported by the Government of Canada through Industry Canada and by the Province of Ontario through the Ministry of Research and Innovation.

[1]C. Strohm, G. L. J. A. Rikken, and P. Wyder, Phys. Rev. Lett. **95**, 155901 (2005).
[2]L. Zhang, J. Ren, J.-S. Wang, and B. Li, Phys. Rev. Lett. **105**, 225901 (2010).
[3]L. Zhang, J. Ren, J.-S. Wang, and B. Li, J. Phys.: Condens. Matter **23**, 305402 (2011).
[4]H. Katsura, N. Nagaosa, and P. A. Lee, Phys. Rev. Lett. **104**, 066403 (2010).
[5]S. Y. Onose *et al.*, Science **329**, 297 (2010).
[6]R. Matsumoto and S. Murakami, Phys. Rev. Lett. **106**, 197202 (2011); Phys. Rev. B **84**, 184406 (2011).
[7]R. Shindou *et al.*, Phys. Rev. B **87**, 174427 (2013); **87**, 174402 (2013).
[8]R. Matsumoto, R. Shindou, and S. Murakami, Phys. Rev. B **89**, 054420 (2014).
[9]I. Dzyaloshinsky, J. Phys. Chem. Solids **4**, 241 (1958); T. Moriya, Phys. Rev. **120**, 91 (1960).
[10]D. J. Thouless, M. Kohmoto, M. P. Nightingale, and M. den Nijs, Phys. Rev. Lett. **49**, 405 (1982); M. Kohmoto, Ann. Phys. **160**, 343 (1985).
[11]H. Lee, J. H. Han, and P. A. Lee, Phys. Rev. B **91**, 125413 (2015).
[12]A. Mook, J. Henk, and I. Mertig, Phys. Rev. B **90**, 024412 (2014); **89**, 134409 (2014).
[13]M. Hirschberger *et al.*, Phys. Rev. Lett. **115**, 106603 (2015).
[14]F. D. M. Haldane, Phys. Rev. Lett. **61**, 2015 (1988).
[15]X. Cao, K. Chen, and D. He, J. Phys.: Condens. Matter **27**, 166003 (2015).
[16]S. A. Owerre, J. Phys.: Condens. Matter **28**, 386001 (2016).
[17]G. Jotzu *et al.*, Nature **515**, 237 (2014).
[18]J. Fransson, A. M. Black-Schaffer, and A. V. Balatsky, e-print arXiv:1512.04902.
[19]A. C. Gossard, V. Jaccarino, and J. P. Remeika, Phys. Rev. Lett. **7**, 122 (1961).
[20]H. L. Davis and A. Narath, Phys. Rev. **134**, A433 (1964).